Solid State Communications 251 (2017) 16–22

Contents lists available at ScienceDirect

Solid State Communications

journal homepage: www.elsevier.com/locate/ssc

Communication

Effects of Li doping on structural, electronic, optical and magnetic properties of $Fe_{0.04}Zn_{0.96}O$ nanocrystalline samples

Md.A. Ahmed[a,*], Mohd Nasir[b], A.K. Yadav[c], A. Banerjee[a,d], S. Bandyopadhyay[a,d]

[a] Department of Physics, University of Calcutta, 92, A.P.C. Road, Kolkata 700009, India
[b] Department of Physics, Indian Institute of Technology Indore, 452020, India
[c] Atomic & Molecular Physics Division, Bhabha Atomic Research Centre, Mumbai 400094, India
[d] Centre for Research in Nanoscience and Nanotechnology, University of Calcutta, Salt Lake, Kolkata 700098, India

ARTICLE INFO

Keywords:
Sol-gel growth
Powder diffraction
Rietveld analysis
Electronic structure
Magnetic properties

ABSTRACT

Sol-gel synthesized nanocrystalline samples of $Li_xFe_{0.04}Zn_{0.96-x}O$ (x = 0.0, 0.02, 0.04 and 0.06) have been investigated through X-ray diffraction (XRD), X-ray absorption near edge spectroscopy (XANES), UV–visible absorption spectroscopy and magnetic measurements. First three samples, i.e., x = 0.0, 0.02 and 0.04, have been found to possess an impurity phase of $ZnFe_2O_4$. As determined from the Rietveld analysis, the presence of $ZnFe_2O_4$ phase has decreased on Li doping and for x = 0.06, it is negligibly small. XANES analysis shows that the majority of Fe ions is in Fe^{3+} state. From the UV–visible spectroscopy, the energy band gap (E_g) of pure ZnO has been estimated to be 3.064 eV, whereas on Fe doping E_g has increased. No significant change in E_g due to Li doping has been observed. Magnetization measurements have revealed that the samples containing $ZnFe_2O_4$ (x = 0.0, 0.02 and 0.04) phase exhibit strong ferromagnetic spin-glass behaviour at low temperature and a weak ferromagnetic ordering at the room temperature. However, the sample with x = 0.06 does not show any significant ferromagnetic ordering in the temperature range of 2–300 K. The observed magnetic ordering and spin-glass behaviour in first three samples have been attributed to the impurity phase of $ZnFe_2O_4$.

1. Introduction

Integrating magnetism with semiconductors to produce spintronic devices [1] has become a very interesting topic [2] in the field of materials research. Such systems can be achieved by adding a minute amount of transition metal (TM) elements to the oxide semiconductors. Such systems, known as diluted magnetic semiconductors (DMSs), can play an important role in future spintronic devices. The simultaneous use of both charge and spin degrees of freedom accommodated into a single material and the interplay between them will explore novel physics and new devices such as spin field-effect transistors, spin light emitting diodes and spin qubits for quantum computers. However, for their practical device applications, these DMS systems must exhibit ferromagnetic ordering above room temperature. Due to its promising electronic and optoelectronic properties, ZnO can be taken as a suitable candidate for realizing such TM doped diluted magnetic oxide (DMO) systems. Dietl et al. [3,4] theoretically predicted that room temperature ferromagnetism could be achieved in TM doped wide-bandgap p-type ZnO by increasing the p-d hybridization and reducing the spin-orbit coupling. However, according to donor impurity band exchange model of Coey et al. [5], ferromagnetic exchanges in wide band gap semiconductors like ZnO, GaN, etc., can be mediated by shallow donor electrons that form bound magnetic polarons (BMPs). These BMPs, in fact, overlap to create a spin-split impurity band. On the other hand, Sato et al. [6] suggested that TM:ZnO would show ferromagnetic ordering only when the carriers produced by TM doping formed a partially filled spin–split impurity band. Following these predictions, a substantial investigation has been done on ZnO based DMOs, and room temperature ferromagnetism has widely been observed in TM (e.g., Mn [7–11], Fe [12–19], Co [5,20,21], Ni [22,23], Cu [24–29] etc.) doped ZnO. Although a number of experimental reports and corresponding mechanisms are available in literature, the actual origin of the magnetic ordering in TM:ZnO systems is still a matter of debate.

Room temperature ferromagnetism in Fe:ZnO has been reported by many groups [12–15]. But the results are conflicting and quite inconsistent. Han et al. were unable to produce room temperature ferromagnetism in pure Fe:ZnO bulk samples prepared by a solid-state reaction method and they suggested that an additional doping of Cu might be necessary to achieve room temperature ferromagnetism in Fe:ZnO [16]. As an alternative mechanism, a double exchange interaction has also been proposed for Fe:ZnO co-doped with Cu [18,19]. However, Shim et al. found that the ferromagnetic ordering in Fe and

* Corresponding author.
E-mail address: azahar24@gmail.com (M.A. Ahmed).

http://dx.doi.org/10.1016/j.ssc.2016.12.010
Received 31 October 2016; Accepted 18 December 2016
Available online 19 December 2016

Cu co-doped ZnO was due to the formation of the secondary phase of $ZnFe_2O_4$ [17]. Therefore, the occurrence of ferromagnetic ordering in Fe:ZnO may be due to metallic clusters and secondary-phase formation or it may have an intrinsic origin. In this present work, we report that the observed ferromagnetism in Fe:ZnO is due to the formation of a secondary phase of $ZnFe_2O_4$. First we prepared Fe:ZnO which contained a small amount of $ZnFe_2O_4$ phase. Then we removed that secondary phase by Li doping. We observed that on diminishing of $ZnFe_2O_4$ phase, the ferromagnetism also vanished. Moreover, a spin-glass behavior in the samples containing $ZnFe_2O_4$ phase was also found. We claim that the simultaneous presence of strong ferromagnetism and spin-glass character in Fe:ZnO is due to the formation of $ZnFe_2O_4$ impurity phase.

2. Experimental procedure

Standard Pechini sol-gel process was used to synthesize nanocrystalline $Li_xFe_{0.04}Zn_{0.96-x}O$ (x = 0.0, 0.02, 0.04 and 0.06) samples. Zinc oxide (ZnO), Lithium nitrate [$LiNO_3$] and Iron nitrate [$Fe(NO_3)_3 \cdot 9H_2O$] were used as precursors. Three separate solutions of (a) Zinc oxide in nitric acid, (b) Lithium nitrate and (c) Iron nitrate in double distilled water were prepared and they were mixed together in appropriate stoichiometric ratios to maintain the doping concentrations of Li and Fe. A solution of citric acid and glycerol was prepared to serve as gelling agent. The gelling agent was added to the mixed aqueous solution of precursors followed by stirring at 80 °C to form a gel which was further dried to produce the powders. These powders were heated at 450 °C to remove the trapped carbonate and nitrate phases. The samples with x = 0.0, 0.02, 0.04 and 0.06 have been denoted by S1, S2, S3 and S4 respectively.

An X-ray diffractometer (PANalytical, XPERT-PRO) with Cu K_α radiation (1.5416 Å) was used to investigate the crystallinity, phase purity and phase quantification. A step size of 0.003° and counting time of 35 s per step were used for all samples. Fullprof 2.05 (2011) program was utilized for Rietveld refinement. The XANES spectra were taken at the Energy-Scanning EXAFS beamline in fluorescence mode at Synchrotron Source (2.5 GeV, 100 mA). The optical absorption spectra were taken by using a UV–Visible spectrometer (PerkinElmer-Lambda35) at room temperature. All magnetic measurements were carried out with a Superconducting Quantum Interference Device Vibrating Sample Magnetometer (SQUID-VSM-050), Quantum Design.

3. Results and discussion

3.1. Structural analysis

XRD patterns of the pure ZnO as well as all doped/co-doped samples are depicted in Fig. 1a. Patterns as obtained from theoretical calculation using Rietveld method are also shown (solid red line) in Fig. 1a. Along with the wurtzite ZnO phase, a secondary phase of $ZnFe_2O_4$ has been detected in the samples S1, S2 and S3 (clearly visible in Fig. 1b shown for sample S1 only) and the peaks at 2θ = 29.9° and 35.2° belong to this secondary phase of $ZnFe_2O_4$. However, in sample S4, no impurity phase of $ZnFe_2O_4$ has been identified in the XRD pattern. From the Rietveld analysis, we have extracted the structural parameters of all samples and they are tabulated in Table 1. It has been found that the pure ZnO has highest unit cell volume and it significantly decreases on 4 at% Fe doping (S1). Apart from the substitutional incorporation of Fe ions into Zn sites with tetrahedral symmetry (FeO_4) and formation of $ZnFe_2O_4$ phase, a fraction of Fe ions can also occupy the interstitial positions with octahedral symmetry (FeO_6) in ZnO lattice. As discussed later (in XANES part), almost all Fe ions are in Fe^{3+} state. Therefore, this decrease in unit cell volume is due to the incorporation of smaller Fe^{3+} ions (ionic radius = 0.49 Å) into Zn^{2+}(ionic radius = 0.60 Å) sites. However, on Li doping, a further decrease in unit cell volume has been observed for sample S2 and then it gradually increases up to sample S4. This clearly indicates that in sample S2, 2 at% Li doping has enhanced Fe^{3+} incorporation into Zn^{2+} site which in turn causes a decrease in unit cell volume. Since, the size of Li^+ ion (ionic radius = 0.59 Å) is comparable to that of Zn^{2+}, therefore, the incorporated Li^+ ions should not change the unit cell volume of ZnO significantly. So, due to increasing Li doping, we must not expect any appreciable change in the unit cell volume. Therefore, in samples S3 and S4, a gradual increase in unit cell volume can be interpreted as the reduction in substitutional incorporation of Fe^{3+} in presence of higher concentration of Li dopant. This might have caused an increase in Fe^{3+} incorporation into the interstitial positions. Another noteworthy point is that the unit cell volumes of all Li and Fe co-doped ZnO samples (S2-S4) are smaller than the unit cell volume of Fe:ZnO (S1). This is an indication of Li assisted higher Fe incorporation into ZnO lattice. But, the trend of increasing unit cell volume as a function of Li doping also puts an upper limit of Li doping to get enhanced Fe incorporation as compared to Fe:ZnO. Phase quantification has also been done from the Rietveld analysis for the samples S1–S4. From Table 1, we observe that the contribution of $ZnFe_2O_4$ phase is highest (5.6%) in sample S1 and it significantly decreases on Li doping. Sample S4 possesses negligibly small amount (~0.01%) of $ZnFe_2O_4$ phase. The average crystallite size has been estimated using the Scherer's formula [30]:

$$D = \frac{K\lambda}{\beta \cos\theta} \quad (1)$$

where the Scherer constant K is taken to be 0.94, λ is the wavelength of the Cu-K_α radiation (1.5416 Å), and β is the full width at half maximum (FWHM-in radians) of the diffraction peak corresponding to the Bragg diffraction angle (2θ). The estimated average crystallite size is given in Table 1. For pure ZnO, the average crystallite size is about 81.2 nm, whereas for samples S1–S4, no much variation (65.8–67.4 nm) has been observed. The observed decrease in average crystallite size can be attributed to the strain produced by the smaller size of Fe dopant in the host ZnO matrix.

3.2. Electronic properties

The oxidation state of doped Fe ions has been investigated by XANES measurement. The XANES spectrum of any element is very sensitive to its oxidation state. Fig. 2 depicts the normalized XANES spectra of all samples (S1–S4) measured at Fe K-edge. For comparison, reference spectra of Fe metal foil (Fe^o), FeO (Fe^{2+}) and Fe_2O_3 (Fe^{3+}) are also shown in Fig. 2. The positions of the main absorption edges of XANES spectra of Fe K-edge of samples S1–S4 are much closed to the reference spectrum of Fe_2O_3. This clearly indicates that the most of the Fe ions in all samples are in Fe^{3+} state. The feature (small peak) before the main absorption edge is called pre-edge. In the inset of Fig. 2, the pre-edges of all XANES spectra of samples S1–S4 are shown in an enlarged view. Pre-edge is a characteristic of transition from Fe:1 s orbital to O:2p-Fe:3d hybridized orbitals. In an isolated Fe atom, the dipole selection rule restricts the transitions from 1 s to 3d orbitals. However, in this present case, this selection rule is not valid for Fe:3d orbitals hybridized with O:2p orbitals in ZnO. Therefore, the presence of the pre-edge peak clearly indicates the hybridization of Fe:3d-O:2p orbitals due to the substitution of Fe ions at Zn sites. Moreover, the area under the pre-edge peak provides a rough estimation of the number of transitions from Fe:1 s to Fe:3d-O:2p hybridized orbitals. From the inset of Fig. 2, the area under the pre-edge peak increases on Li doping. This may be due to the increasing concentration of Li^+(hole dopant) ions which in turn generates a fraction of Fe ions with higher oxidation states. Fe ions with higher oxidation states will have more empty Fe:3d-O:2p hybridized orbitals and therefore, the number of transitions should also increase.

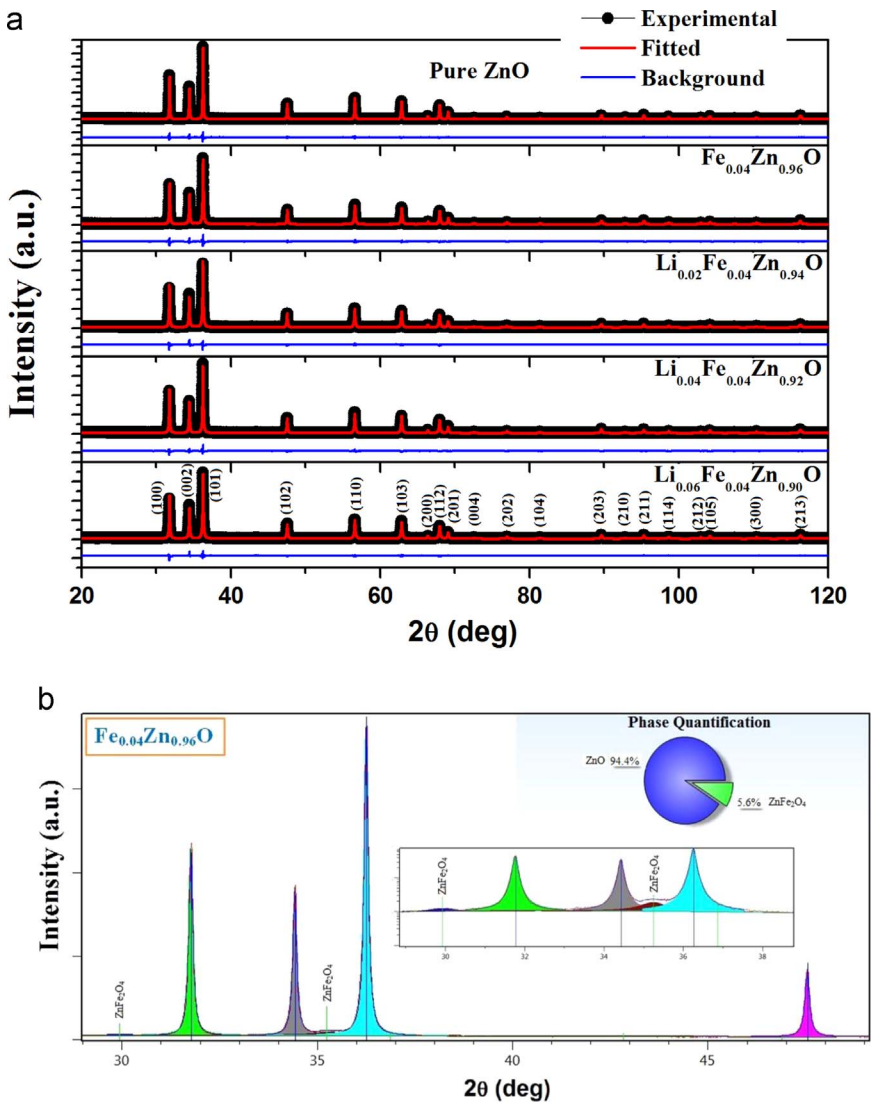

Fig. 1. (Color online) a. XRD patterns of pure ZnO as well as all doped/co-doped samples. b. XRD plot of sample S1 in the range of 2θ = 29–49°. Inset shows the same plot in logarithmic scale. The peaks at 29.9° and 35.2° correspond to $ZnFe_2O_4$ phase.

3.3. UV–visible absorption spectroscopy

The energy band gap (E_g) of the pure ZnO as well as all doped/co-doped samples S1–S4 has been estimated using UV–visible absorption spectroscopy. For a direct band gap semiconductor (e.g., ZnO), Tauc equation [31] can be written as,

$$\alpha h\nu = A(h\nu - E_g)^{1/2} \quad (2)$$

where hν, α and A are photon energy, absorption coefficient and a constant respectively. The plots of $(\alpha h\nu)^2$ versus hν are depicted in

Table 1
Structural parameters, crystallite size and optical energy band gap of pure and all doped/co-doped ZnO samples.

Parameters		Samples				
		ZnO	$Fe_{0.04}Zn_{0.96}O$	$Li_{0.02}Fe_{0.04}Zn_{0.94}O$	$Li_{0.04}Fe_{0.04}Zn_{0.92}O$	$Li_{0.06}Fe_{0.04}Zn_{0.90}O$
Space group		$P6_3mc$	$P6_3mc$	$P6_3mc$	$P6_3mc$	$P6_3mc$
Symmetry		Tetrahedral	Tetrahedral	Tetrahedral	Tetrahedral	Tetrahedral
$a=b$ (Å)		3.2499	3.2499	3.2497	3.2497	3.2498
c (Å)		5.2061	5.2057	5.2051	5.2055	5.2055
V (Å^3)		47.6213	47.6154	47.6042	47.6083	47.6105
χ^2		2.19	1.75	1.56	1.48	1.57
R_p		10.5	10.6	9.56	8.90	12.2
R_{wp}		12.1	11.5	10.5	9.93	11.8
R_{exp}		8.16	8.72	8.43	8.15	9.45
Phase contribution	ZnO	100%	94.40%	97.49%	98.99%	99.99%
	$ZnFe_2O_4$	–	5.60%	2.51%	1.01%	0.01%
Crystallite size (nm)		81.2	66.7	65.9	65.8	67.4
Band gap (eV)		3.064	3.150	3.149	3.150	3.157

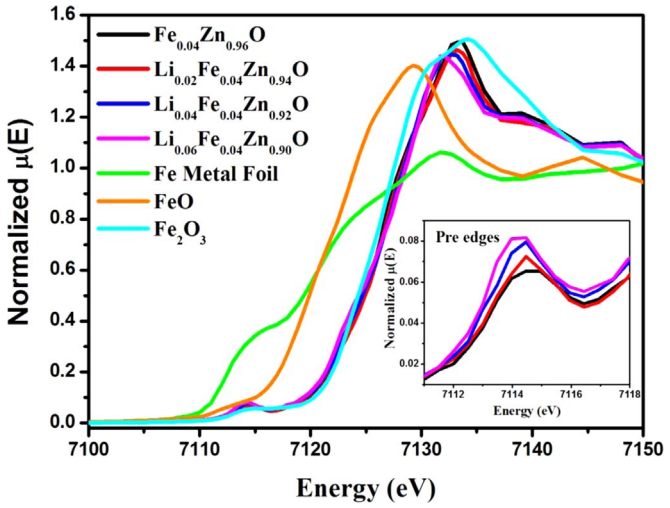

Fig. 2. (Color online) XANES spectra of all doped/co-doped samples measured at Fe K-edge along with the reference spectra of Fe metal foil, FeO and Fe_2O_3. Inset shows the enlarged view of pre-edge peaks.

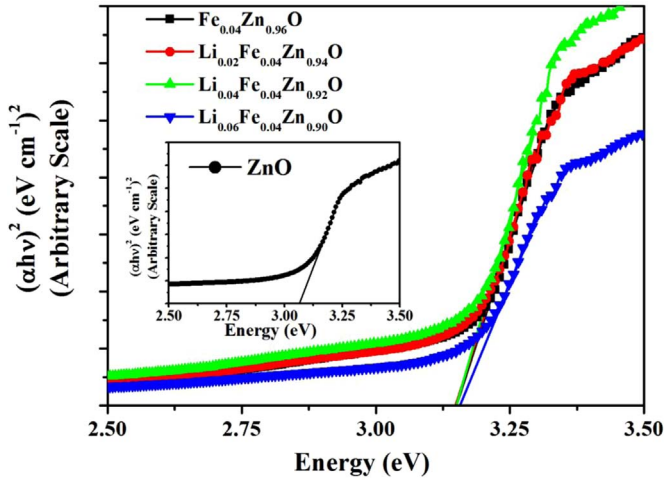

Fig. 3. (Color online) UV–visible absorption spectra of all doped/co-doped samples. Inset shows the same spectrum of pure ZnO.

Fig. 3. E_g is estimated by extrapolating the linear region of each plot. The results are given in Table 1. We find that the pure ZnO has E_g value of 3.064 eV and this observed red shift in E_g (as compared to 3.4 eV [32]) can be explained as follows: ZnO is an n-type polar semiconductor. Due to the presence of various intrinsic defects in ZnO, a significant number of electron-hole pairs can generate at room temperature. Because of the polar nature of ZnO, a moving electron in the conduction band and a hole in the valence band attract the oppositely charged ions and constitute polarons which modify the self-energy and cause a downward shift due to many-body interactions [33,34]. On 4 at %Fe doping, $E_g$increases as compared to our pure ZnO and it remains almost unchanged for samples S1–S4. No significant change in E_g due to Li doping has been observed. This increase in E_g (as compared to our pure ZnO) due to Fe doping can be interpreted in terms of Burstein-Moss effect [34–36]. If one Fe^{3+} ion substitutionally replaces one Zn^{2+} ion, then one extra electron goes to the conduction band of ZnO and occupies one energy state. Therefore, due to 4 at% Fe doping, a significant number of electrons can populate the lower energy levels in the conduction band of ZnO and hence the energy gap (E_g) between the top of the valence band maximum and the lowest unoccupied energy level of the conduction band gets increased.

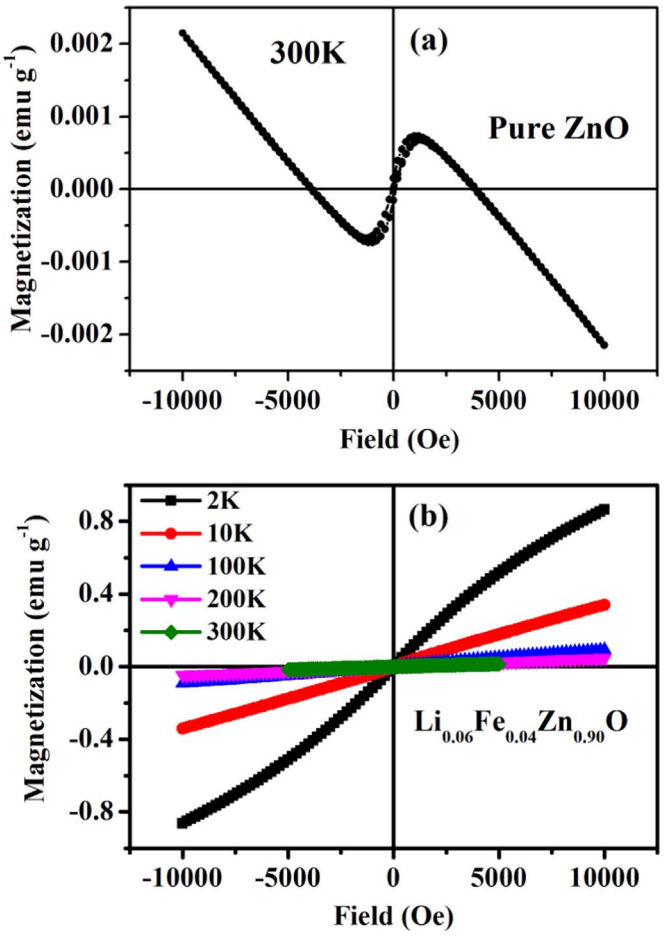

Fig. 4. (Color online) Field dependent magnetization (M-H) of (a) pure ZnO at 300 K and (b) sample S4 at 2, 10, 100, 200, and 300 K.

3.4. Magnetic studies

Room temperature magnetization as a function field (M-H) of the pure ZnO sample is presented in Fig. 4a. A pure and defectless ZnO is a diamagnetic material. But in our case, we observe that our pure ZnO exhibits ferromagnetic behavior at low field region whereas it is diamagnetic at high field region. This observed ferromagnetic behavior can be attributed to the presence of intrinsic defects in ZnO such as Zinc vacancies (V_{Zn}), Zinc interstitials (I_{Zn}), Oxygen vacancies (V_O), Oxygen interstitials (I_O) etc. The defect induced bound magnetic polaron (BMP) model [5] is often used to explain such ferromagnetic behavior.

Temperature dependent magnetization (M-T) under zero field cooled (ZFC) and field cooled (FC) conditions at 300 Oe has been recorded for samples S1–S4. The M-T variations are illustrated in Fig. 5(a–d). In samples S1–S3, there is a pronounced peak in all ZFC curves and this feature indicates the presence of spin-glass or super-paramagnetic behavior. However, in sample S4, no such peak in the ZFC curve has appeared. In the XRD analysis, we found that the samples S1–S3 contained impurity phase of $ZnFe_2O_4$, whereas, the sample S4 was found to have negligibly small amount of $ZnFe_2O_4$ phase. Therefore, we can say that the observed spin-glass or super-paramagnetic nature in samples S1–S3 is due to the $ZnFe_2O_4$ impurity phase. Another notable feature in the M-T curves is the gradual appearance of paramagnetic dominance at the lower temperature region with Li doping. This may be due to the increment of the number of isolated paramagnetic (non-interacting) Fe ions in the system. Li

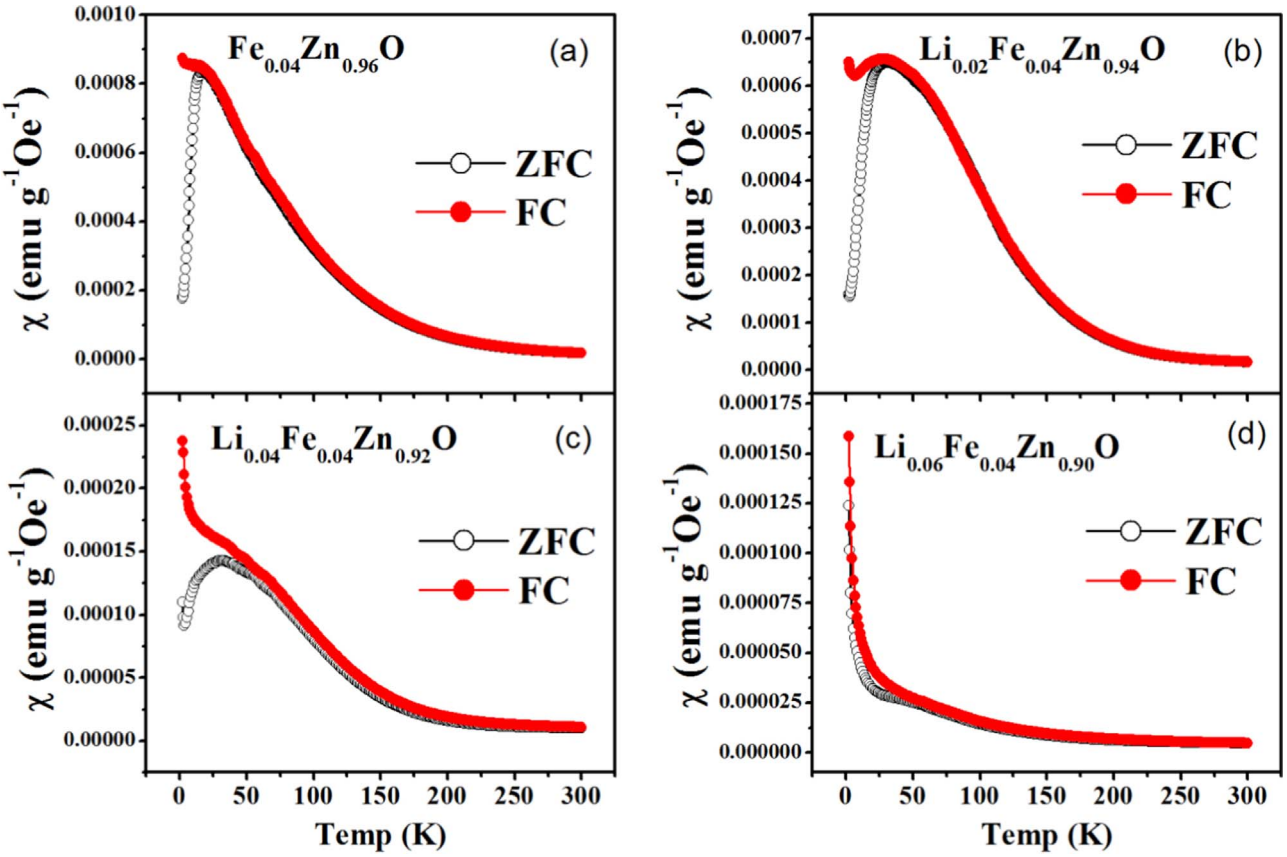

Fig. 5. (Color online) Temperature dependent magnetization (ZFC and FC) of samples (a) S1, (b) S2, (c) S3, and (d) S4.

ions might have played a role in destroying ferromagnetic coupling of some of the Fe ions. These Fe ions are well separated from one another and hence they do not contribute to the ferromagnetic coupling through direct or indirect exchange interactions. These Fe ions behave as isolated magnetic impurities in Li rich ZnO and lead to the paramagnetic contribution.

Fig. 4b shows the M-H variations of sample S4 in the temperature range of 2–300 K. No noticeable strong ferromagnetic hysteresis loop has appeared in any of the M-H curves. However, in the samples S1–S3, we have observed strong ferromagnetic ordering with well-defined hysteresis loop (coercivity ~1110 Oe) at 2 K and with significantly small hysteresis loop (coercivity ~27–79 Oe) at higher temperatures. As shown in Fig. 6a (small paramagnetic contribution subtracted), all four samples (S1–S4) exhibit weak ferromagnetic ordering at room temperature (300 K). The variation of the saturation moment (M_S) as a function of Li content is depicted in the inset of Fig. 6a. The observed decrease in M_S with increase of Li content is definitely due to the removal of $ZnFe_2O_4$ impurity phase on Li doping. Out of remaining three samples (S1–S3), M-H curves (small paramagnetic contribution subtracted) at different temperatures are presented only for sample S1 in Fig. 6b. Other two samples (S2 and S3) show similar M-H behavior and therefore, they are not presented here. The sample S1 exhibits significantly high coercivity (~1110 Oe) as well as remnant magnetization (~0.363 emu/g) at 2 K as compared to elevated temperatures (coercivity ~27–79 Oe and remnant magnetization ~0.0086–0.066 emu/g). This implies that the sample S1 (and also S2–S3) behaves as a hard ferromagnet at 2 K and as a soft ferromagnet at higher temperatures. The presence of a strong ferromagnetic ordering in samples S1–S3, and the absence in sample S4, can simply be attributed to the impurity phase of $ZnFe_2O_4$.

In order to investigate the nature (spin-glass or superparamagnetic) of $ZnFe_2O_4$, we have performed ac susceptibility measurement (at 3 Oe ac field) at different frequencies for sample S1. The temperature dependent variations of the real part (χ′) as well as the imaginary part (χ″) of the ac susceptibility (χ_{ac}) at different frequencies are shown in Fig. 6c and d respectively. In case of a spin-glass, a frequency dependent sharp peak (cusp) is observed in both the components χ′ and χ″ of χ_{ac}. The position of the peak in χ′ is defined as the freezing temperature (T_f), which coincides with the point of inflection in χ″ (insets of Fig. 6c and d). In χ′, the peak shifts towards the lower temperature side and its intensity increases as the frequency of the ac field is decreased. However, in case of χ″, the peak shifts towards the lower temperature side and its intensity decreases with decreasing ac frequency. This kind of frequency dependent responses of χ′ and χ″ components of χ_{ac} are a typical feature of spin-glass systems. To further verify the spin-glass behavior, the value of the quantity $\Delta T_f/[T_f \log(\omega)]$ has been calculated. For spin glass systems, this quantity varies in the range of 0.004–0.018 [37] whereas for superparamagnetic systems, it is of the order of 0.3 [37]. In our case, we have found that the quantity lies in the range of 0.006–0.02 which is consistent for a system to be spin-glass. Another evidence for spin-glass character can be provided from the nature of the low field region of the virgin branch of M-H curve at 2 K (inset of Fig. 6b). The curve shows an S shape with positive curvature at the low field region which is a signature of spin-glass systems [38].

4. Conclusion

Effects of Li doping on sol-gel synthesized $Fe_{0.04}Zn_{0.96}O$ nanocrystalline sample have been investigated in this work. The impurity phase of $ZnFe_2O_4$ in $Fe_{0.04}Zn_{0.96}O$ has been removed gradually by increasing concentration of Li doping. XANES analysis has revealed that the most of the Fe ions are in Fe^{3+} state in all doped/co-doped samples. $Fe_{0.04}Zn_{0.96}O$ shows a higher energy band gap (3.150 eV) as compared to our pure ZnO (3.064 eV). However, Li doping does not show any significant effect on the energy band gap. The samples containing

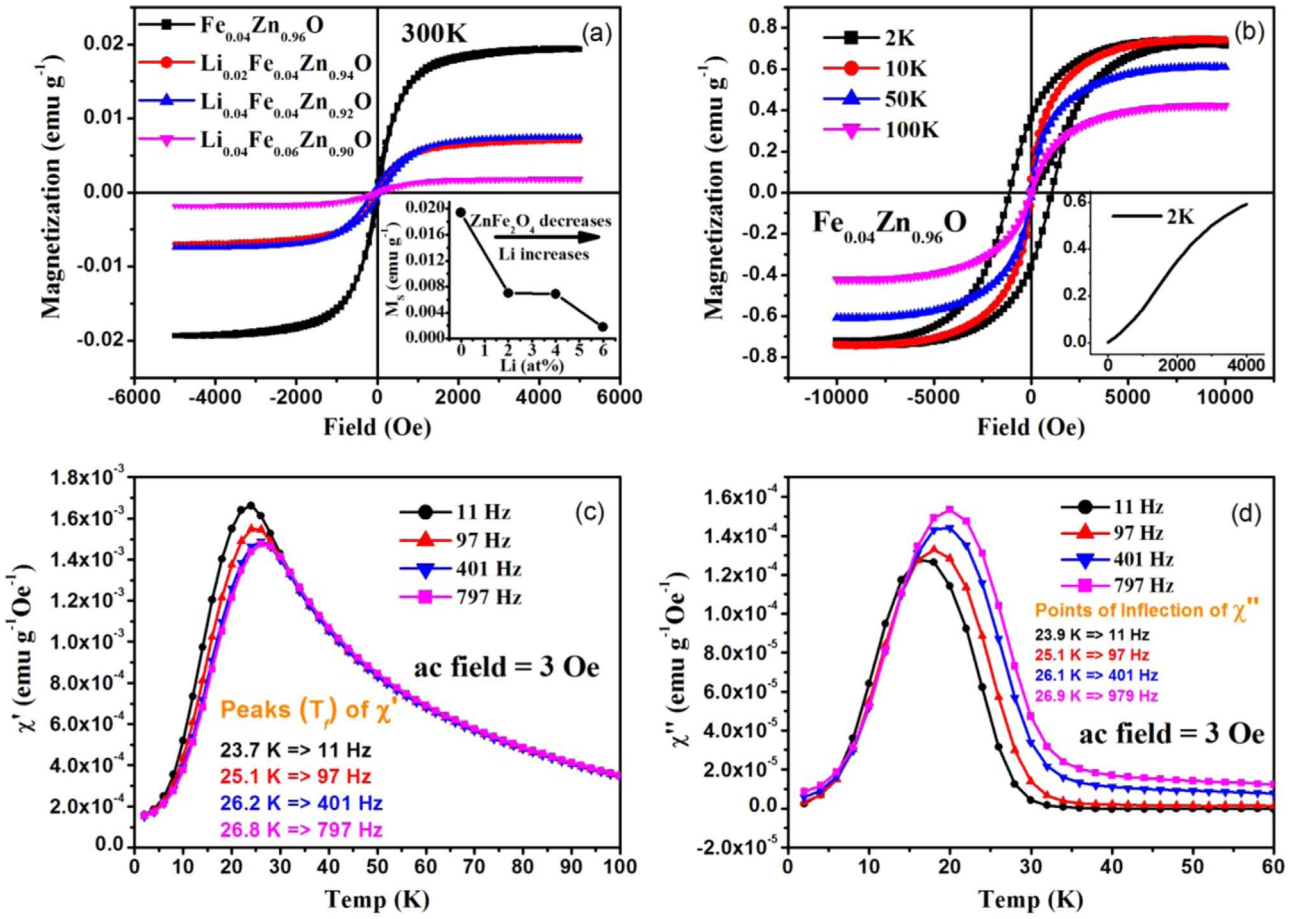

Fig. 6. (Color online) (a) M-H variations of samples S1–S4 at 300 K, (b) M-H variations of sample S1 at different temperatures, (c) Real part of ac susceptibility at different frequencies, and (d) Imaginary part of ac susceptibility at different frequencies.

$ZnFe_2O_4$ phase show strong ferromagnetic ordering at low temperature whereas at room temperature the ferromagnetic strength is weak. However, the sample free from $ZnFe_2O_4$ phase exhibits weak ferromagnetic ordering at all temperatures. We claim that the observed magnetic ordering in the samples (up to 4 at% Li doped) is due to the presence of $ZnFe_2O_4$ impurity phase. The spin-glass nature of $ZnFe_2O_4$ has also been established through magnetic measurements.

Acknowledgement

The author Md. A. Ahmed is thankful to the University Grants Commission (UGC), New Delhi, India, for providing Maulana Azad National Fellowship (award letter no. MANF-2012-13-MUS-WES-18230). We acknowledge Raja Ramanna Centre for Advanced Technology (RRCAT), Indore, India, for providing the synchrotron facility for XANES measurement. We acknowledge UGC DAE CSR, KC, India for financial support through CRS.

References

[1] S.A. Wolf, D.D. Awschalom, R.A. Buhrman, J.M. Daughton, S. von Molnár, M.L. Roukes, A.Y. Chtchelkanova, D.M. Treger, Science 294 (2001) 1488.
[2] Y. Matsumoto, M. Murakami, T. Shono, T. Hasegawa, T. Fukumura, M. Kawasaki, P. Ahmet, T. Chikyow, S. Koshihara, H. Koinuma, Science 291 (2001) 854.
[3] T. Dietl, H. Ohno, F. Matsukura, J. Cibert, D. Ferrand, Science 287 (2000) 1019.
[4] T. Dietl, Semicond. Sci. Technol. 17 (2002) 377.
[5] J.M.D. Coey, M. Venkatesan, C.B. Fitzgerald, Nat. Mater. 4 (2005) 173.
[6] K. Sato, H. Katayama-Yoshida, Jpn. J. Appl. Phys. 39 (2000) L555.
[7] D.C. Kundaliya, S.B. Ogale, S.E. Lofland, S. Dhar, C.J. Metting, S.R. Shinde, Z. Ma, B. Varughese, K.V. Ramanujachary, L. Salamanca-riba, T. Venkatesan, Nat. Mater. 3 (2004) 709.
[8] P. Sharma, A. Gupta, K.V. Rao, Frank J. Owens, R. Sharma, R. Ahuja, J.M. Osorio Guillen, B. Johansson, G.A. Gehring, Nat. Mater. 2 (2003) 673.
[9] W. Yan, Z. Sun, Q. Liu, Z. Li, Z. Pan, J. Wang, S. Wei, D. Wang, Y. Zhou, X. Zhang, Appl. Phys. Lett. 91 (2007) 062113.
[10] D.P. Norton, S.J. Pearton, A.F. Hebard, N. Theodoropoulou, L.A. Boatner, R.G. Wilson, Appl. Phys. Lett. 82 (2003) 239.
[11] S.Y. Park, P.J. Kim, Y.P. Lee, S.W. Shin, T.H. Kim, J.H. Kang, Adv. Mater. 19 (2007) 3496.
[12] A. Sahai, Y. Kumar, V. Agarwal, S.F. Olive-Méndez, N. Goswami, J. Appl. Phys. 116 (2014) 164315.
[13] Q. Wang, Q. Sun, P. Jena, Y. Kawazoe, Phys. Rev. B 79 (2009) 115407.
[14] A.Y. Polyakov, A.V. Govorkov, N.B. Smirnov, N.V. Pashkova, S.J. Pearton, K. Ip, R.M. Frazier, C.R. Abernathy, D.P. Norton, J.M. Zavada, R.G. Wilson, Mater. Sci. Semicond. Process. 7 (2004) 77.
[15] K. Potzger, S.Q. Zhou, H. Reuther, A. Mu cklich, F. Eichhorn, N. Schell, W. Skorupa, M. Helm, J. Fassbender, Appl. Phys. Lett. 88 (2006) 052508.
[16] S.J. Han, J.W. Song, C.H. Yang, S.H. Park, J.H. Park, Y.H. Jeong, Appl. Phys. Lett. 81 (2002) 4212.
[17] J.H. Shim, T. Hwang, S. Lee, Appl. Phys. Lett. 86 (2005) 082503.
[18] M.S. Park, B.I. Min, Phys. Rev. B 64 (2001) 100403 (R).
[19] M.S. Park, B.I. Min, Phys. Rev. B 68 (2003) 224436.
[20] Y. Belghazi, G. Schmerber, S. Colis, J.L. Rehspringer, A. Dinia, A. Berrada, Appl. Phys. Lett. 89 (2006) 122504.
[21] M. Venkatesan, C.B. Fitzgerald, J.G. Lunney, J.M.D. Coey, Phys. Rev. Lett. 93 (2004) 177206.
[22] X. Liu, F. Lin, L. Sun, W. Cheng, X. Ma, W. Shi, Appl. Phys. Lett. 88 (2006) 062508.
[23] T. Wakano, N. Fujimura, Y. Morinaga, N. Abe, A. Ashida, T. Ito, Physica E 10 (2001) 260.
[24] C. Xu, J. Chun, D. Kim, B. Chon, T. Joo, Appl. Phys. Lett. 91 (2007) 153104.
[25] D.B. Buchholz, R.P.H. Chang, J.H. Song, J.B. Ketterson, Appl. Phys. Lett. 87 (2005) 082504.
[26] C. Sudakar, J.S. Thakur, G. Lawes, R. Naik, V.M. Naik, Phys. Rev. B 75 (2007) 054423.
[27] D.L. Hou, X.J. Ye, H.J. Meng, H.J. Zhou, X.L. Li, C.M. Zhen, G.D. Tang, Appl. Phys. Lett. 90 (2007) 142502.
[28] T.S. Herng, S.P. Lau, S.F. Yu, H.Y. Yang, X.H. Ji, J.S. Chen, N. Yasui, H. Inaba, J. Appl. Phys. 99 (2006) 086101.
[29] D.L. Hou, X.J. Ye, X.Y. Zhao, H.J. Meng, H.J. Zhou, X.L. Li, C.M. Chen, J. Appl. Phys. 102 (2007) 033905.
[30] C. Chen, B. Yu, J. Liu, Q. Dai, Y. Zhu, Mater. Lett. 61 (2007) 2961.
[31] J. Tauc, R. Grigorvici, Y. Yanca, Phys. Status Solidi 15 (1966) 627.

[32] D.C. Look, Mater. Sci. Eng. B 80 (2001) 383.
[33] B.E. Sernelius, Phys. Rev. B 36 (1987) 4878.
[34] B.E. Sernelius, K.F. Berggren, Z.C. Jin, I. Hamberg, C.G. Granqvist, Phys. Rev. B 37 (1988) 10244.
[35] E. Burstein, Phys. Rev. 93 (1954) 632.
[36] T.S. Moss, Proc. Phys. Soc. B 76 (1954) 775.
[37] J.A.Mydosh, Spin glasses: an experimental introduction (Taylor & Francis, London, 1993.
[38] C.A. Cardoso, F.M. Araujo-Moreira, V.P.S. Awana, E. Takayama-Muromachi, O.F. de Lima, H. Yamauchi, M. Karppinen, Phys. Rev. B 67 (2003) 020407 (R).